Capillarity

Vol. 6, No. 1, p. 13-18, 2023

Original article

CO_2 adsorption and separation properties of M-MOF-74 materials determined by molecular simulation

Jia Deng, Guangjie Zhao, Lan Zhang*, Huizhong Ma, Yan Rong

School of Mechanics and Safety Engineering, Zhengzhou University, Zhengzhou 450001, P. R. China

Keywords:
Metal-organic frameworks
M-MOF-74 materials
adsorption
separation
molecular simulation

Cited as:
Deng, J., Zhao, G., Zhang, L., Ma, H., Rong, Y. CO_2 adsorption and separation properties of M-MOF-74 materials determined by molecular simulation. Capillarity, 2023, 6(1): 13-18.
https://doi.org/10.46690/capi.2023.01.02

Abstract:
This study simulated the adsorption and separation of CO_2 by the metal-organic frameworks material M-MOF-74, established the skeleton model of M-MOF-74 series adsorbent, and calculated the adsorption of CO_2 pure component gas and CO_2/N_2 mixed gas on M-MOF-74 series adsorbent by the grand canonical Monte Carlo method. Among the CO_2 adsorption performances of MOF-74 materials with metal centers of Mg, Co, Ni, and Zn, Mg-MOF-74 had the highest CO_2 adsorption capacity, adsorption selection coefficient and adsorption heat. When mixed gas was adsorbed, the law of CO_2 adsorption was consistent with that of pure CO_2 adsorption. The size law of adsorption heat on MOF-74 was similar to that of adsorption amount. Our findings demonstrated that the interaction between the metal-organic framework material and CO_2 is greater than that between the material and N_2. The interaction between the gas and the MOF-74 series adsorbent was the main factor affecting the adsorption amount, which reveals the strong influence of metal central atoms on the amount of gas adsorption. Our findings provide new ideas for the design of efficient adsorbent materials.

1. Introduction

In the face of the global increase in atmospheric CO_2 levels, various materials have been proposed for CO_2 adsorption, while most of these are targeted at major CO_2 emission sites with high CO_2 concentrations such as chemical plants, iron works, thermal power plants, etc. (Zhen et al., 2012; Meconi and Zangi, 2020). However, with the development of the global economy, the number of cars is increasing day by day and they account for 9.2% of total CO_2 emissions (Sun et al., 2022). The research and development of materials that absorb low-concentration CO_2 from automobile exhausts to control carbon dioxide emissions is of great significance for carbon neutralization and global warming (Hua and Dong, 2022).

Compared with activated carbon, zeolite and other solid adsorbents, metal-organic frameworks have higher adsorption selectivity (Pham et al., 2016; Singh et al., 2020). The technology of carbon capture and storage is widely used to greatly expand the selection range of adsorbents. Among the variety of material structures, those from the M-MOF-74 series can effectively adsorb CO_2 due to their open metal sites, which has been proved for CO_2 capture (Millward and Yaghi, 2005; Kuppler et al., 2009; Liu et al., 2012). Caskey (Caskey et al., 2008) found that a huge amount of CO_2 was adsorbed by Mg-MOF-74 whose adsorption capacity could reach 8.6 mmol/g for CO_2 under conditions of 298 K and 1 bar, and their open metal sites significantly affected CO_2 adsorption capacity and selectivity. Yazaydın and Bae (Yazaydın et al., 2009; Bae and Long, 2013) screened 14 kinds of MOFs for low-pressure CO_2 adsorption and separation, and found that MOFs with open metal sites could adsorb a large amount of CO_2 under low pressure, much higher than other types of MOFs. A large number of studies have demonstrated that MOFs exhibit improved CO_2 adsorption performance due to their open metal sites, thus are widely utilized in CO_2 adsorption and separation.

Herein, molecular dynamics simulation was used to estab-

Yandy Scientific Press

*Corresponding author.
E-mail address: dengjialucky@zzu.edu.cn (J. Deng); zgj15690632798@163.com (G. Zhao); ielzhang@zzu.edu.cn (L. Zhang); iehzma@zzu.edu.cn (H. Ma); rongyan@zzu.edu.cn (Y. Rong).

Received November 29, 2022; revised December 24, 2022; accepted January 10, 2023; available online January 13, 2023.

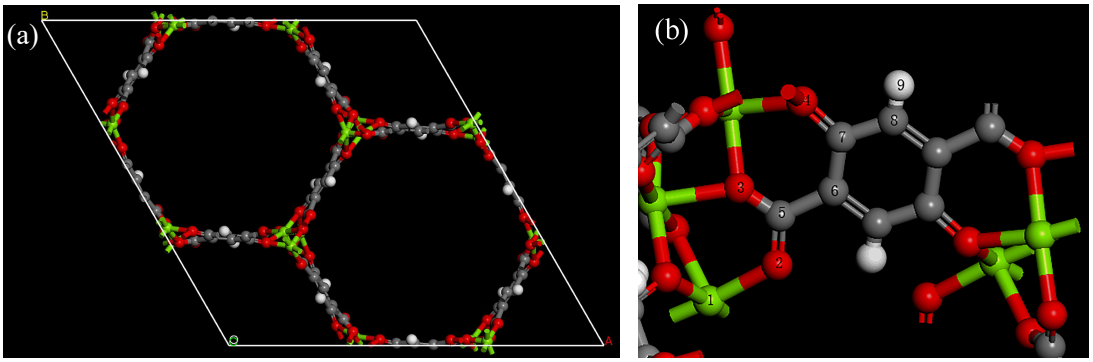

Fig. 1. Schematic diagram of the Mg-MOF-74 model: (a) Framework model and (b) atom distribution.

Table 1. Charge of each atom in the M-MOF-74 model (Yazaydın et al., 2009).

No.	Charge (e)			
	Mg-MOF-74	Zn-MOF-74	Co-MOF-74	Ni-MOF-74
1	1.458	1.206	1.139	1.100
2	-0.714	-0.670	-0.684	-0.677
3	-0.909	-0.659	-0.645	-0.623
4	-0.784	-0.702	-0.731	-0.679
5	0.800	0.767	0.832	0.789
6	-0.260	-0.292	-0.292	-0.239
7	0.492	0.325	0.315	0.358
8	-0.280	-0.147	-0.110	-0.201
9	0.197	0.172	0.176	0.172

Table 2. L-J potential parameters of atoms in M-MOF-74 (Mayo et al., 1990; Rappe et al., 1992).

Atomic type	σ (Å)	ε/kB (K)
C	3.898	47.856
H	3.195	7.649
O	3.405	48.158
Zn	4.054	27.677
Mg	3.021	55.857
Co	2.872	7.045
Ni	2.834	7.548

Table 3. CO_2 and N_2 model parameters (Potoff and Siepmann, 2001; Yu et al., 2015).

Parameters	CO_2		N_2	
Charge (e)	C	0.7	N	0
	O	-0.35	-	-
Bond distances (Å)	C=O	1.175	N≡N	1.105
Bond angle	O=C=O	179.983°	N≡N	180°

lish a model for evaluating the adsorption and separation performances of M-MOF-74 materials for CO_2 and N_2. Based on this model, the effects of the open metal sites of M-MOF-74 materials on their CO_2 performance indicators, such as adsorption selectivity, adsorption capacity, and adsorption heat, were examined.

2. Methodology

2.1 Model

The crystal structure of Mg-MOF-74 was determined according to the Cambridge Crystallographic Data Centre. M-MOF-74 materials (M = Mg, Zn, Co, Ni) can be obtained by appropriately adding, deleting and modifying some atoms (Dietzel et al., 2005). Fig. 1 demonstrates the framework model and atom distribution of Mg-MOF-74 with the following lattice parameters: $a = b$ = 2.611 nm, c = 0.672 nm, $\alpha = \beta = 90°$, $\gamma = 120°$.

Table 1 illustrates the charge distribution of each atom in the M-MOF-74 model shown in Fig.2(b), and Table 2 presents the Lennard Jones (L-J) parameters for the atoms in M-MOF-74. The interaction energy of each atom E in the system is derived from the Coulomb and L-J potential equation:

$$E_{ij} = 4\varepsilon_{ij}\left[\left(\frac{\sigma_{ij}}{\gamma_{ij}}\right)^{12} - \left(\frac{\sigma_{ij}}{\gamma_{ij}}\right)^{6}\right] + \frac{q_i q_j}{4\pi\varepsilon_0\gamma_{ij}} \quad (1)$$

where γ_{ij} denotes the distance between particles; σ_{ij} means the depth of potential well; ε_{ij} represents the depth of potential energy; q is the charge of atoms; ε_0 is the vacuum dielectric constant that is equal to 8.8542×10^{-12} $C^2/(N*m^2)$. Based on the Lorentz-Berthelot (L-B) mixing rules, the cross-terms were employed for calculating the L-J potential function.

Fig. 2 presents the schematic diagram of the CO_2 and N_2 models, and the model parameters are shown in Table 3.

2.2 Computational methods

The GCMC simulation was implemented based on Materials Studio (Akkermans et al., 2013), and the Universal For-

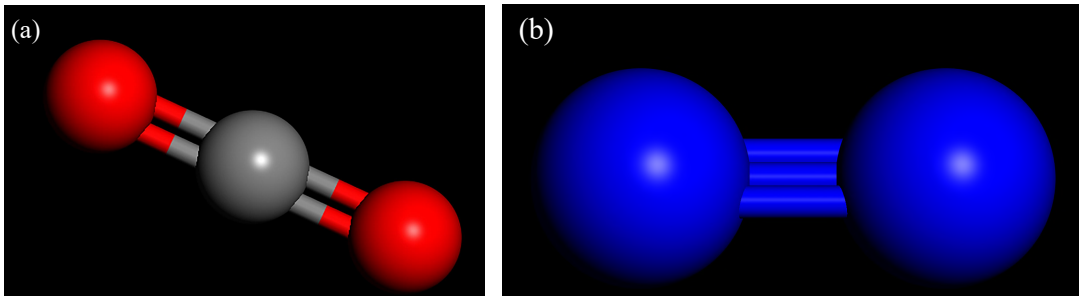

Fig. 2. Schematic diagram of the CO_2 and N_2 models: (a) CO_2 and (b) N_2.

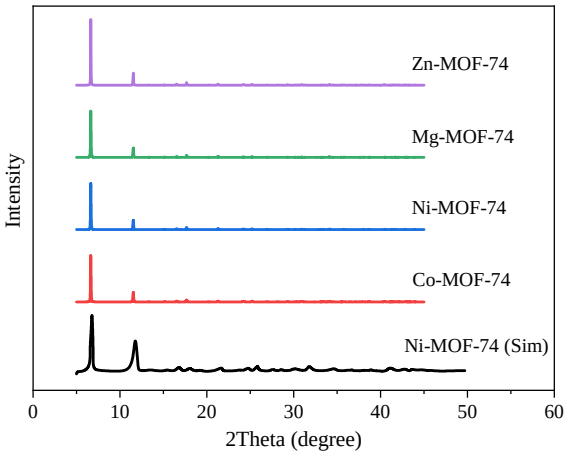

Fig. 3. Comparison of simulated and experimental XRD patterns of M-MOF-74.

ce Field was employed in the GCMC simulation (Yang et al., 2018). The skeleton material was regarded as a rigid structure in the simulation, and van der Waals interaction force was calculated using the atom-based method and described by using L-J potential function. Periodic boundary conditions were adopted, and the cut-off radius was 12.8 Å. The Ewald addition method was implemented for calculating the electrostatic interactions. The interaction of different particles was calculated by L-B mixing rules. The modeling was carried out in a total of 3×10^6 steps. Herein, the first 1.5×10^6 steps were employed for systematic equilibrium, and the last 1.5×10^6 steps were adopted for the calculation of adsorption data.

2.3 Model and verification

Fig. 3 compares the simulated X-Ray Diffraction (XRD) pattern of M-MOF-74 and the experimental XRD pattern of Ni-MOF-74 (Chen et al., 2015). For the XRD pattern (2θ = 5-50°), the experimental XRD pattern shows good agreement with the simulated XRD pattern. The optimized Mg-MOF-74 cell constants are $a = b = 2.61102$ nm, and $c = 0.67192$ nm. The simulated cell volume $V = 3.9669$ nm^3 ($a = b = 2.602$ nm, $c = 0.672$ nm, $V = 3.941$ nm^3) is within 1% error compared with the data (Caskey et al., 2008). Table 4 shows the specific surface area of the M-MOF-74 material model, which is slightly larger than that obtained in the experiment (Choi et al., 2017), because the model is ideal and there may

Table 4. M-MOF-74 specific surface area.

Model	Simulation (m^2/g)	Experiment (m^2/g) *
Mg-MOF-74	1,851.04	1,525
Zn-MOF-74	1,422.38	1,134
Co-MOF-74	1,466.55	1,356
Ni-MOF-74	1,451.33	1,239

* from Choi et al. (2017).

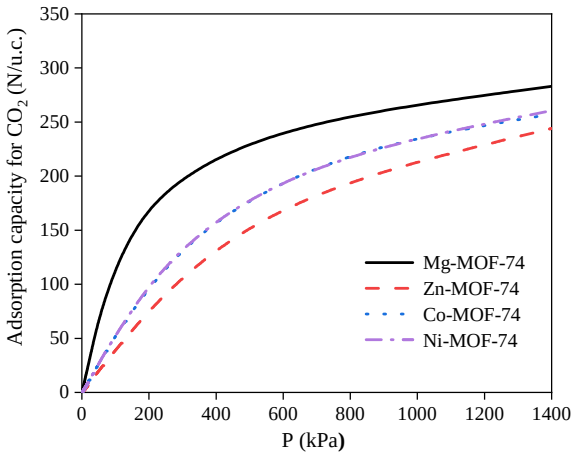

Fig. 4. CO_2 adsorption isotherm curves of M-MOF-74.

be impurities in the synthesized MOFs. Thus, it is inferred that the model established in this paper has high reliability and can be simulated in the next step.

3. Results and discussion

3.1 Adsorption performance of M-MOF-74 for pure CO_2

With reference to the effect of different metal central atoms on the amount of CO_2 adsorption, the CO_2 capacity adsorbed by M-MOF-74 was calculated under the conditions of 298 K and 0-1,200 kPa. This work presents the adsorption capacity, adsorption site and adsorption heat of the system as the performance indicators.

Fig. 4 illustrates the adsorption isotherm curves of four metal-organic framework materials. The adsorption isotherms

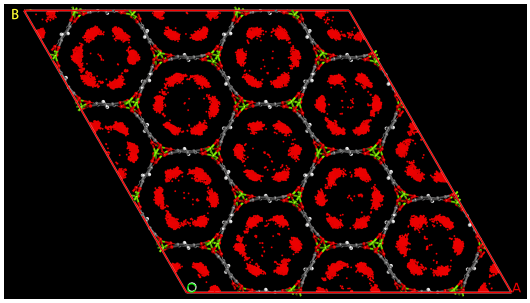

Fig. 5. Diagram of adsorption points.

of the 4 MOFs have the same trend, which belong to the type I isotherm. At the initial stage, the amount of CO_2 adsorption rises rapidly in the lower pressure range due to the presence of metal adsorption sites, where CO_2 can be preferentially adsorbed. However, with the pressure increasing, the rising curve of CO_2 adsorption capacity tends to be flat. Due to the increase in adsorption capacity, the preferential adsorption sites in MOF-74 materials are gradually filled, and the framework is gradually occupied by CO_2 gas. Thus, the interaction between the gas and the framework is weakened. Among the four materials, Mg-MOF-74 has the largest specific surface area and pore volume. At the initial stage of adsorption, the gas molecules can obtain a larger contact area and storage space (Bergmann et al., 2015); therefore, the CO_2 adsorption capacity with regard to the four framework materials is in the descending order of Mg-MOF-74 > Co-MOF-74 ≈ Ni-MOF-74 > Zn-MOF-74.

In order to further understand the adsorption position of CO_2 molecules in the metal-organic frameworks, the adsorption locations of the Mg-MOF-74 were illustrated in Fig. 5, where the red dots represent the adsorption points of CO_2. According to the diagram of adsorption points, it is concluded that CO_2 molecules are first adsorbed near these bare metal sites, and there are a few scattered adsorption sites at the center of the framework pore. This indicates that, for M-MOF-74, the adsorption of CO_2 by the framework materials is mainly determined by the interaction of different metal centers for CO_2 molecules.

Adsorption heat represents the thermal effect in the adsorption process of adsorbate, which is caused by the reduction in the molecular motion speed of gas molecules, the reduction in kinetic energy and the release of heat in the adsorption process. Adsorption heat is an important index to measure the strength of adsorption capacity of the adsorbent, and its value reflects the strength of interaction between adsorbent material and gas. The CO_2 adsorption heat with regard to M-MOF-74 is illustrated in Fig. 6, where Mg-MOF-74 has the largest heat from CO_2 adsorption and the order of CO_2 adsorption heat basically corresponds to the order of adsorption capacity. Mg-MOF-74 has the strongest interaction with CO_2, while Zn-MOF-74 has the weakest.

3.2 Adsorption performance of M-MOF-74 for CO_2/N_2

Fig. 7 shows the CO_2/N_2 (15/85 v/v%) adsorption of M-MOF-74, where the ratio of CO_2 to N_2 is 15:85 (Yang et al., 2012; Yang et al., 2018). The addition of N_2 molecules can reduce the amount of CO_2 adsorption, and the CO_2 adsorption capacity of the four skeleton materials is in the descending order of Mg-MOF-74 > Co-MOF-74 ≈ Ni-MOF-74 > Zn-MOF-74, as shown in Fig. 7(a). The adsorption capacity for N_2 is smaller than that for CO_2 because the unsaturated metal site in the adsorbate has a strong adsorption ability for gas molecules with a large quadrupole distance. When comparing the quadrupole moments of CO_2 and N_2, that of CO_2 is larger than N_2. Hence, the interaction of the material with N_2 is small, and the N_2 adsorption capacity of 4 skeleton materials is in the descending order of Mg-MOF-74 ≈ Zn-MOF-74 > Co-MOF-74 ≈ Ni-MOF-74, as demonstrated in Fig. 7(b).

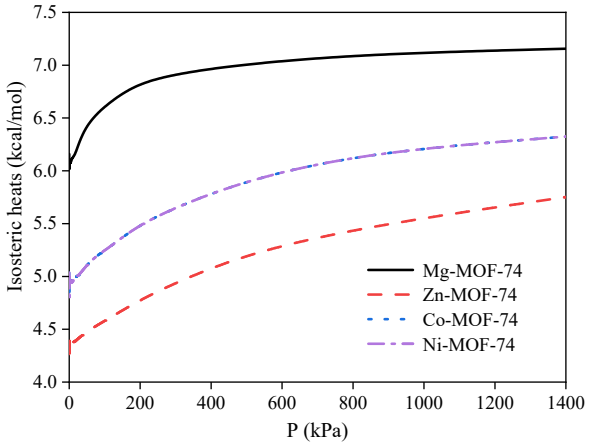

Fig. 6. The adsorption heat of CO_2 for M-MOF-74.

To further analyze the difference in the CO_2 adsorption capacity of M-MOF-74 (M = Mg, Zn, Co, Ni) under two-component CO_2/N_2 gas, the adsorption locations of the Mg-MOF-74 were shown in Fig. 8. Here, Fig. 8(a) demonstrates the adsorption locations of CO_2 on Mg-MOF-74, and Fig. 8(b) illustrates the adsorption locations of CO_2 and N_2 molecules on Mg-MOF-74, where the red dots represent the adsorption points of CO_2 and the green dots stand for the adsorption points of N_2. Based on the distribution of adsorption sites, it is inferred that when N_2 molecules are added, they can replace some preferential CO_2 adsorption sites, and some open sites are switched to adsorb N_2 instead of CO_2. Hence, CO_2 is partly dispersed in the skeleton. Due to the presence of N_2 molecules, the CO_2 adsorption capacity of Mg-MOF-74 is reduced as some of the adsorption sites can no longer adsorb this molecule.

The selective adsorption coefficient is used to calculate the influence of the components with different partial pressures on the adsorption capacity of the mixed system, which is an important parameter used for evaluating the separation performance of the mixed gas.

The adsorption selectivity coefficient S is calculated as follows:

$$S_{1/2} = \frac{x_1/x_2}{y_1/y_2} \tag{2}$$

where subscript 1 and 2 denote CO_2 and N_2, respectively; x_1 and x_2 represent the molar components of two components in the adsorption phase, respectively; y_1 and y_2 stand for the mo-

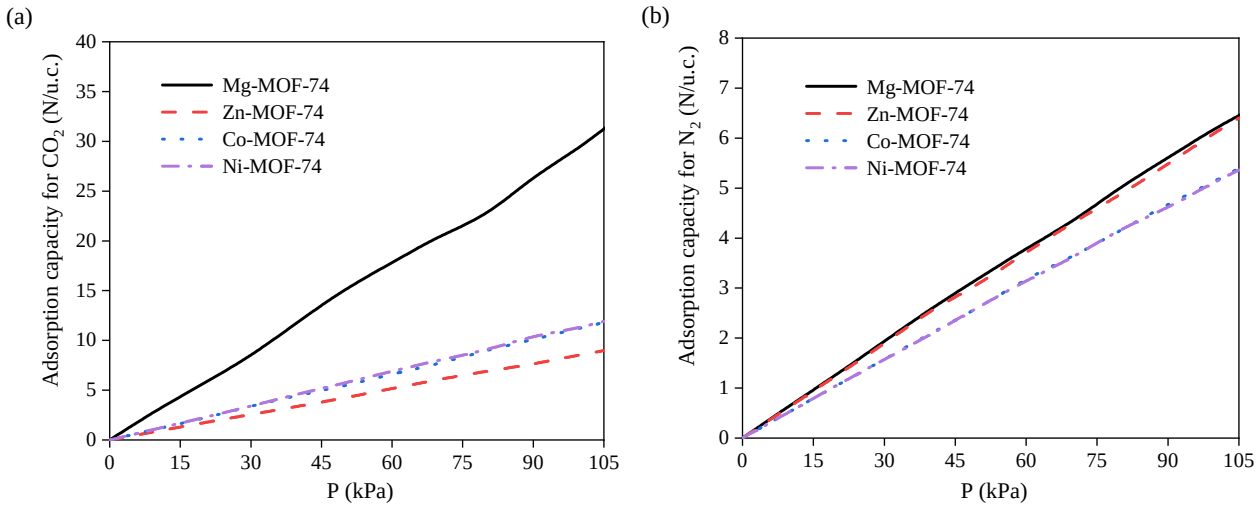

Fig. 7. CO_2 and N_2 adsorption of M-MOF-74: (a) CO_2 and (b) N_2.

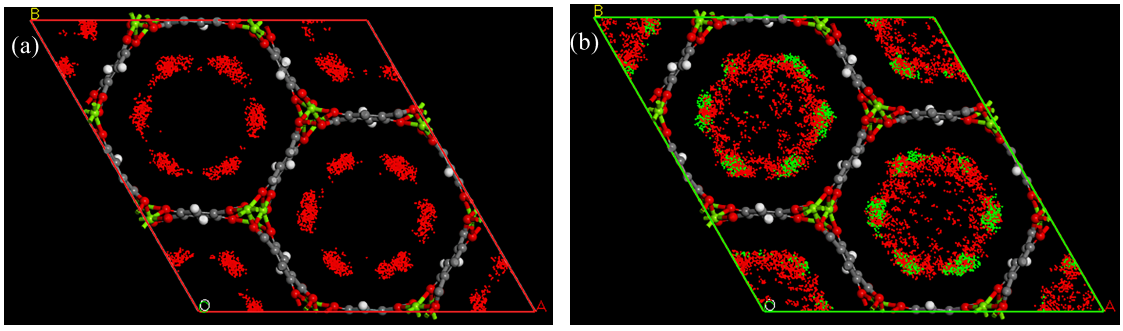

Fig. 8. Diagram of adsorption points: (a) CO_2 and (b) CO_2/N_2.

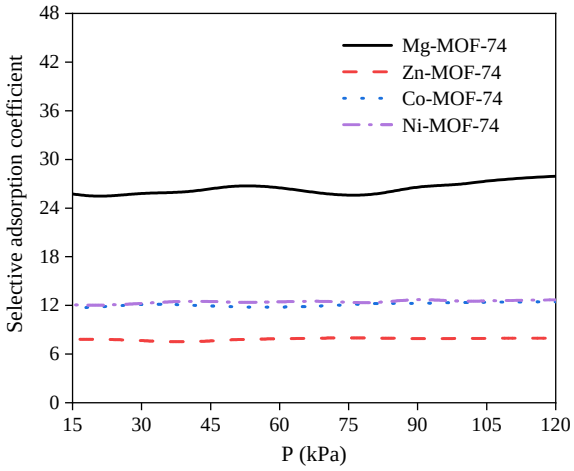

Fig. 9. Selective adsorption coefficient of M-MOF-74.

lar components of two components in the gas phase, respectively.

The adsorption selectivity coefficients of the four adsorbent materials for the mixed gas are further calculated, as shown in Fig. 9. The selectivity coefficients of all materials are greater than 1, indicating that M-MOF-74 has a selective adsorption effect for CO_2 in the mixed gas and the interaction between CO_2 gas and materials is strong; therefore, CO_2 will be preferentially adsorbed. Among the four materials, Mg-MOF-74 has the highest CO_2 selective adsorption coefficient, while Zn-MOF-74 has the lowest. Under the condition of 100 kPa and 298 K, the CO_2 selective adsorption coefficient of the four skeleton materials is in the descending order of Mg-MOF-74 > Ni-MOF-74 > Co-MOF-74 > Zn-MOF-74.

4. Conclusions

In the present work, a molecular dynamics simulation method was developed to establish a M-MOF-74 model, which was used to investigate the CO_2 adsorption performances of MOF-74 materials with metal centers of Mg, Co, Ni and Zn and their selectivity for CO_2/N_2. Among the four materials, Mg-MOF-74 had the highest CO_2 adsorption capacity, adsorption selection coefficient and adsorption heat. In comparison with the adsorption capacity of pure CO_2 and the selectivity of mixed gas in M-MOF-74 series materials, Mg-MOF-74 had the best adsorption and separation performance. It was also highlighted that the gas is mainly adsorbed near the metal central atom of M-MOF-74, the amount of adsorption is affected by the interaction between the metal central atom and the gas, and the interaction between them could be expressed by the heat of adsorption. This study revealed the influence of

metal central atoms on the amount of gas adsorption, thereby providing some ideas for the design of efficient adsorbent materials.

Acknowledgements

The work was supported by National Natural Science Foundation of China (No. 11602227) and the Key Scientific Research Project for Colleges and Universities in Henan Province (No. 22A130007).

Conflict of interest

The authors declare no competing interest.

References

Akkermans, R. L. C., Spenley, N. A., Robertson, S. H. Monte Carlo methods in materials studio. Molecular Simulation, 2013, 39(14-15): 1153-1164.

Bae, T., Long, J. R. CO_2/N_2 separations with mixed-matrix membranes containing Mg2(dobdc) nanocrystals. Energy & Environmental Science, 2013, 6(12): 3565-3569.

Bergmann, J., Stein, K., Kobalz, M., et al. A series of isomorphous metal-organic frameworks with rtl topology-Metal distribution and tunable sorption capacity via substitution of metal ions. Microporous and Mesoporous Materials: The Offical Journal of the International Zeolite Association, 2015, 216: 56-63.

Caskey, S. R., Wong-Foy, A. G., Matzger, A. J. Dramatic tuning of carbon dioxide uptake via metal substitution in a coordination polymer with cylindrical pores. Journal of the American Chemical Society, 2008, 130(33): 10870-10871.

Chen, D. L., Shang, H., Zhu, W., et al. Reprint of: Transient breakthroughs of CO_2/CH_4 and C_3H_6/C_3H_8 mixtures in fixed beds packed with Ni-MOF-74. Chemical Engineering Science, 2015, 124: 109-117.

Choi, I., Jung, Y. E., Yoo, S. J., et al. Facile synthesis of M-MOF-74 (M = Co, Ni, Zn) and its application as an electrocatalyst for electrochemical CO_2 conversion and H_2 production. Journal of Electrochemical Science and Technology, 2017, 8(1): 61-68.

Dietzel, P. D. C., Morita, Y., Blom, R., et al. An in situ high-temperature single-crystal investigation of a dehydrated metal-organic framework compound and field-induced magnetization of one-dimensional metal-oxygen chains. Angewandte Chemie International Edition, 2005, 44(39): 6354-6358.

Hua, Y., Dong, F. How can new energy vehicles become qualifed relays from the perspective of carbon neutralization? Literature review and research prospect based on the CiteSpace knowledge map. Environmental Science and Pollution Research, 2022, 29: 55473-55491.

Kuppler, R. J., Timmons, D. J., Fang, Q., et al. Potential applications of metal-organic frameworks. Coordination Chemistry Reviews, 2009, 253(23-24): 3042-3066.

Liu, Y., Wang, Z., Zhou, H. Recent advances in carbon dioxide capture with metal-organic frameworks. Greenhouse Gases: Science and Technology, 2012, 2(4): 239-259.

Mayo, S. L., Olafson, B. D., Goddard, W. A. DREIDING: A generic force field for molecular simulations. The Journal of Physical Chemistry, 1990, 94(26): 8897-8909.

Meconi, G. M., Zangi, R. Adsorption-induced clustering of CO_2 on graphene. Physical Chemistry Chemical Physics, 2020, 22: 21031-21041.

Millward, A. R., Yaghi, O. M. Metal-organic frameworks with exceptionally high capacity for storage of carbon dioxide at room temperature. Journal of the American Chemical Society, 2005, 127(51): 17998-17999.

Pham, T. H., Lee, B. K., Kim, J., et al. Enhancement of CO_2 capture by using synthesized nano-zeolite. Journal of the Taiwan Institute of Chemical Engineers, 2016, 64: 220-226.

Potoff, J. J., Siepmann, J. I. Vapor-liquid equilibria of mixtures containing alkanes, carbon dioxide, and nitrogen. AIChE Journal, 2001, 47(7): 1676-1682.

Rappe, A. K., Casewit, C. J., Colwell, K. S., et al. UFF, a full periodic table force field for molecular mechanics and molecular dynamics simulations. Journal of the American Chemical Society, 1992, 114(25): 10024-10035.

Singh, G., Lee, J., Karakoti, A., et al. Emerging trends in porous materials for CO_2 capture and conversion. Chemical Society Reviews, 2020, 49: 4360-4404.

Sun, X., Sun, L., Zhang, H., et al. The progress of foreign automobile carbon emission standards and its enlightenment to China. China Standardization, 2022, 11: 77-83. (in Chinese)

Yang, J., Ding, Y., Liao, Q., et al. CO_2 adsorption and separation in Br-group-modified Mg-MOF-74. Journal of Thermal Science and Technology, 2018, 17(3): 185-190. (in Chinese)

Yang, X., Feng, L., Wei, P., Automobile exhaust pollution and its harm. Frontier Science, 2012, 6(3): 10-22. (in Chinese)

Yazaydın, A. Ö., Snurr, R. Q., Park, T. H., et al. Screening of metal-organic frameworks for carbon dioxide capture from flue gas using a combined experimental and modeling approach. Journal of the American Chemical Society, 2009, 131(51): 18198-18199.

Yu, J., Balbuena, P. B. How impurities affect CO_2 capture in metal-organic frameworks modified with different functional groups. ACS Sustainable Chemistry & Engineering, 2015, 3(1): 117-124.

Zhen, L., Lu, W., Kong, X., et al. Onsite CO_2 capture from flue gas by an adsorption process in a coal-fired power plant. Industrial & Engineering Chemistry Research, 2012, 51(21): 7355-7363.